ADVANCED MATERIALS

Supporting Information

for *Adv. Mater.*, DOI 10.1002/adma.202312207

Linearly Interlinked Fe-N_x-Fe Single Atoms Catalyze High-Rate Sodium-Sulfur Batteries

Jiufeng Ruan, Yao-Jie Lei, Yameng Fan, Marcela Chaki Borras, Zhouxin Luo, Zichao Yan, Bernt Johannessen, Qinfen Gu, Konstantin Konstantinov, Wei Kong Pang, Wenping Sun, Jia-Zhao Wang, Hua-Kun Liu, Wei-Hong Lai*, Yun-Xiao Wang* and Shi-Xue Dou*

Supporting Information

Linearly Interlinked Fe-N_x-Fe Single Atoms Catalyze High-Rate Sodium-Sulfur Batteries

Jiufeng Ruan, Yao-Jie Lei, Yameng Fan, Marcela Chaki Borras, Zhouxin Luo, Zichao Yan, Bernt Johannessen, Qinfen Gu, Konstantin Konstantinov, Wei Kong Pang, Wenping Sun, Jia-Zhao Wang, Hua-Kun Liu, Wei-Hong Lai,* Yun-Xiao Wang,* Shi-Xue Dou*

Experimental section

Preparation of Fe/NC/700, Fe/NC/600 and Fe/NC/800

Zeolitic imidazolate framework-8 (ZIF-8) nanoparticles were synthesized using a previously reported room-temperature rapid synthesis method. Firstly, 2.61 g of $Zn(NO_3)_2 \cdot 6H_2O$ and 5.74 g of 2-methylimidazole (purchased from Sigma without further purification) were separately dissolved in 87 ml of methanol each. The solutions were then mixed in a beaker and vigorously stirred for an hour. Next, the resulting ZIF-8 nanoparticles were separated from the solution through centrifugation at 8,000 rpm for 3 min, washed three times with methanol solution, dried in a blast oven, and ground for further use.

The prepared ZIF-8 particles were pyrolyzed in a tube furnace at 300℃ for 2 h and at 700°C for 2 h with a heating rate of 5℃ min^{-1} under flowing nitrogen gas (research grade, BOC Ltd) to obtain nitrogen-doped carbon frameworks (NC/700-Zn). To remove Zn residue after pyrolysis and obtain NC/700-N, the product was refluxed in a 2 M H_2SO_4 solution (95% H_2SO_4, Sigma) for 12-15 h at 60℃, as leaching Zn under aggressive acid reflux conditions was found to be significantly more effective than leaching at room temperature. In the second step, 100 mg of NC/700-N powder was dispersed in 100 ml of methanol (VWR) containing 64 mg of $FeCl_2$ (99%, Sigma) and then refluxed for 12-15 h at 60℃ with constant stirring. Next, it was filtered in de-ionized water three times and then dried in a vacuum oven overnight at 70℃ to yield NC/700-Fe. To prevent aggregation of Fe atoms during subsequent heating, an extra N source, dicyandiamide, was introduced to immobilize Fe atoms in the precursor. The dried powder was mixed with dicyandiamide (DCDA, 99%, Sigma-Aldrich) in a weight ratio of 2:1 and thoroughly ground for 15 min before being subjected to the next step,

which involved heating at 700℃ for 1 h with a heating rate of 5℃ min^{-1} under flowing 5% H_2/Ar gas mixture (BOC Ltd) to obtain Fe/NC/700. To synthesize Fe/NC/600 and Fe/NC/800, the same synthesis steps were followed as for Fe/NC/700, with the only difference being the temperature at which they were heated during the pyrolysis step. Specifically, ZIF-8 particles were heated to 600℃ and 800℃ to obtain NC/600-Zn and NC/800-Zn, respectively. After doping with DCDA, the annealing temperature was adjusted to 600℃ and 800℃, respectively, to obtain Fe/NC/600 and Fe/NC/800. The Fe mass loading of Fe/NC/600, Fe/NC/700, and Fe/NC/800 was about 5 wt%, as measured by inductively coupled plasma-optical emission spectroscopy (ICP-OES).

Preparation of S@Fe/NC

Fe/NC/600, Fe/NC/700, and Fe/NC/800 were each mixed with S powder in a weight ratio of 1:1.5, and sealed in separate quartz ampoules. The sealed quartz tubes were then annealed at 155℃ for 12 hours, after which, the temperature was raised to 300℃ and held for 2 hours, using a melt and diffusion approach, to obtain S@Fe/NC/600, S@Fe/NC/700, and S@Fe/NC/800, respectively.

Electrochemical performance measurements

The electrochemical tests were conducted by assembling half-cells in an argon-filled glove box. A slurry of 70% active materials (S@Fe/NC/700), 15% carbon black, and 15% carboxymethyl cellulose (CMC) was prepared with an appropriate amount of deionized water. The slurry was then coated on Cu foil and dried in a vacuum oven at 55℃ overnight. The electrodes were subsequently punched to form round disks with diameters of 0.97 cm, and the average mass loading was between 1.5-2 $mg \cdot cm^{-2}$. The preparation procedures for high mass loading of sulfur cathode are as follows. We punched copper foil into round disks with diameters of 0.97cm first and then apply the slurry onto the electrode sheet. The procedure for preparing high-loading sulfur cathode sheets involves uniformly mixing the active material with CMC and carbon black in a 7:1.5:1.5 ratio using a mortar and pestle. Subsequently, DI water is incrementally added into the mixture for three times with hand grinding for about 0.5 hours until achieving a fine slurry. After coating the slurry on the Cu discs, the electrodes are placed in a 50℃-vacuum oven overnight. Before assembling the coin cells, the electrode discs are pressed at 10MPa using a hydraulic press to ensure tight attachment of the active material on the Cu foil. Sodium foil was used for both the reference and counter electrode, while glass fibre was selected as the separator. The Na-S batteries were assembled using an electrolyte consisting of 1 M $NaClO_4$ in ethylene carbonate (EC)/propylene carbonate (PC) with a 1:1 volume ratio. The electrochemical measurements were conducted on a NEWARE coin cell

tester in a constant temperature chamber at 25℃, and a Biologic VMP-3 electrochemical workstation within the voltage range of 0.8–2.8 V, with all capacities normalized by the weight of S.

Physicochemical characterization

The morphology was investigated with a field emission scanning electron microscope (FESEM, JEOLJSM-7500FA) and a 200 kV scanning transmission electron microscope (STEM, JEM-ARM 200F). For the high-angle annular dark-field (HAADF) observations, the angular range of collected electrons was about 70-250 mrad and an STEM-annular bright field (ABF) detector was used to collect ABF-STEM images. The energy dispersive spectroscopy (EDS) mapping was derived using NSS software. The XRD patterns were detected via a PAN analytical diffractometer with Cu Kα radiation at the scan rate of 0.02° s^{-1}. X-ray photoelectron spectroscopy (XPS) was conducted with Al Kα radiation in fixed analyzer transmission mode: the pass energy was 60 eV for the survey spectra and 20 eV for the specific elements. The nitrogen absorption and desorption isotherms were obtained at 77.3 K using a Quadrasorb-evoTM analyzer. The thermal decomposition behavior of the products was monitored by employing a Mettler Toledo TGA/SDTA851 analyzer, heating them from 50℃ to 700°C in an Ar atmosphere at a rate of 5°C min^{-1}. Time-of-Flight Secondary Ion Mass Spectrometry (TOF-SIMS) measurements were performed in the negative mode using a TESCAN MAIA3 instrument. An electrode was subjected to a pulsed 30 keV Ga^{+} (3nA) ion beam. The TOF-SIMS measurements were conducted across an electrode sample volume with a 100 µm x 100 µm sputtering area and approximately 2 µm sputtered depth. This electrode surface was selected after a full discharge to 0.8 V. X-ray absorption spectroscopy (XAS) experiments were carried out at the applied X-ray absorption fine structure spectroscopy (XAFS) beamline at the Australian Synchrotron in Melbourne. The obtained XAFS data was processed in Athena (version 0.9.26) for background, pre-edge line, and post-edge line calibrations. Then, a Fourier transformed fitting was carried out in Artemis (version 0.9.26). *In-situ* XRD was conducted at the Powder Diffraction Beamline, Australian Synchrotron (ANSTO). The wavelength was 0.6877 Å using the NIST LaB6 660b standard reference material. The inductively coupled plasma-optical emission spectroscopy (ICP-OES) was measured by Perkin Elmer ICP Avio 500.

Supplementary Figures

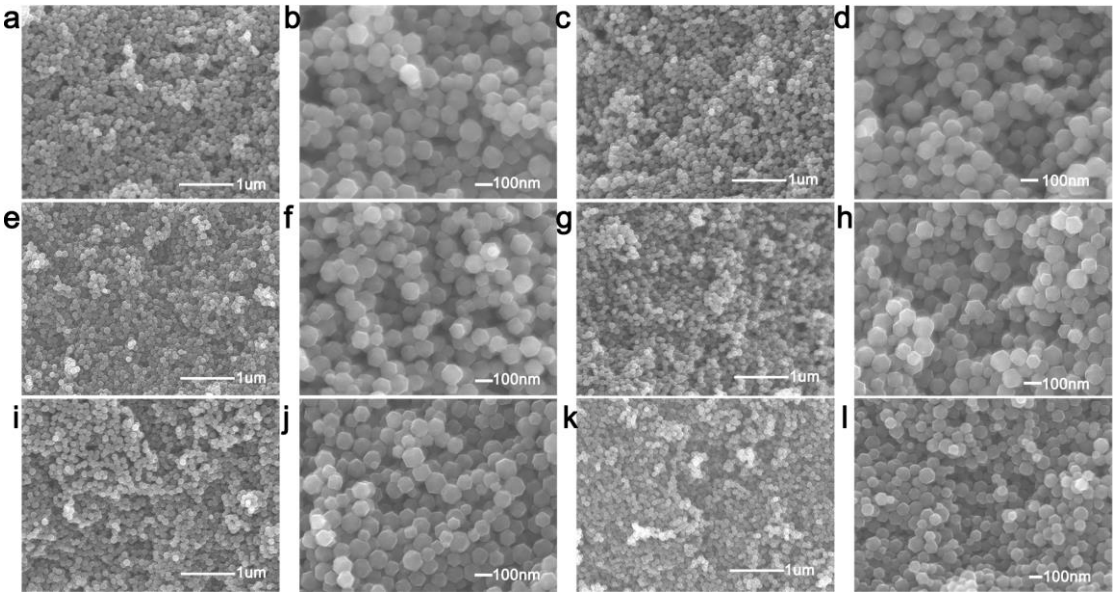

Figure S1. SEM images of (a-b) Fe/NC/600, (c-d) S@Fe/NC/600, (e-f) Fe/NC/700, (g-h) S@Fe/NC/700, (i-j) Fe/NC/800, (k-l) S@Fe/NC/800. The average particle size for all these six samples is about 90nm.

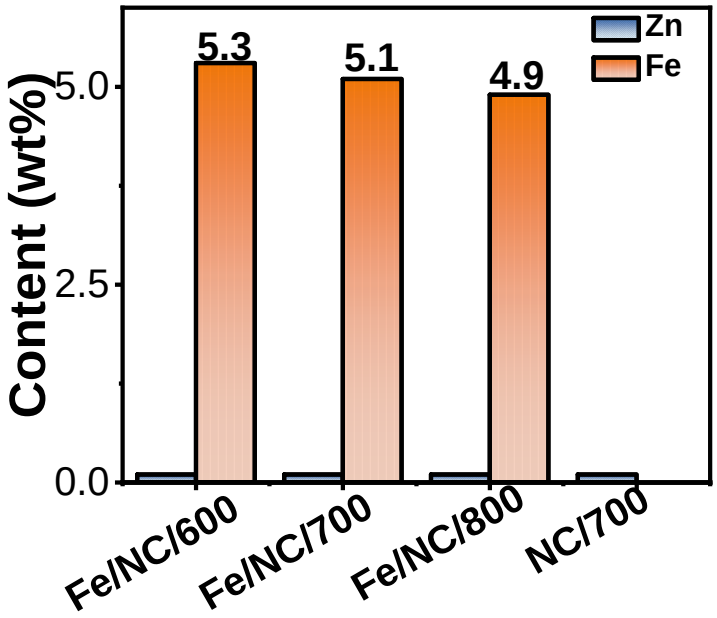

Figure S2. ICP results for Fe/NC/600, Fe/NC/700, Fe/NC/800, and NC/700.

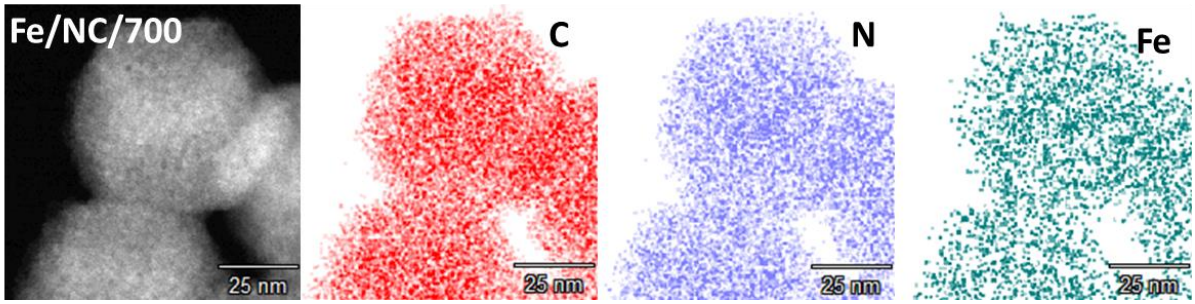

Figure S3. EDS mapping of Fe/NC/700.

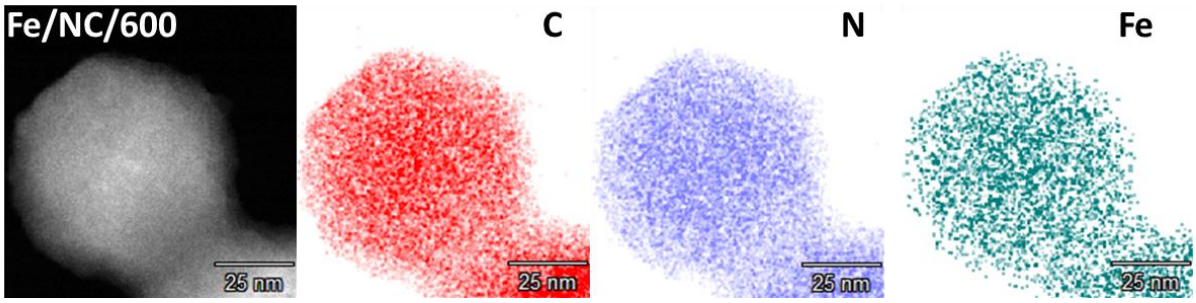

Figure S4. EDS mapping of Fe/NC/600.

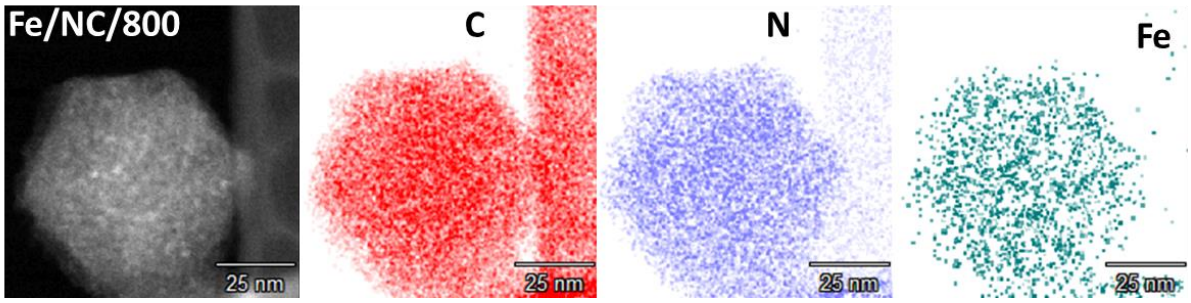

Figure S5. EDS mapping of Fe/NC/800.

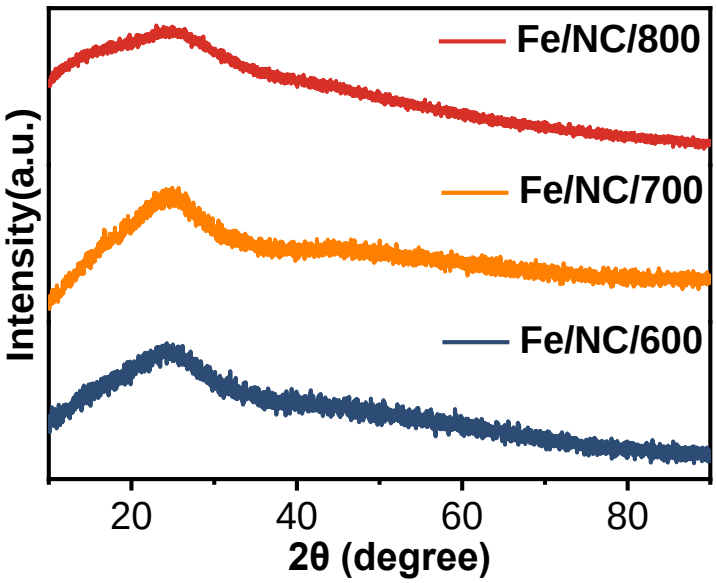

Figure S6. XRD of Fe/NC/600, Fe/NC/700 and Fe/NC800.

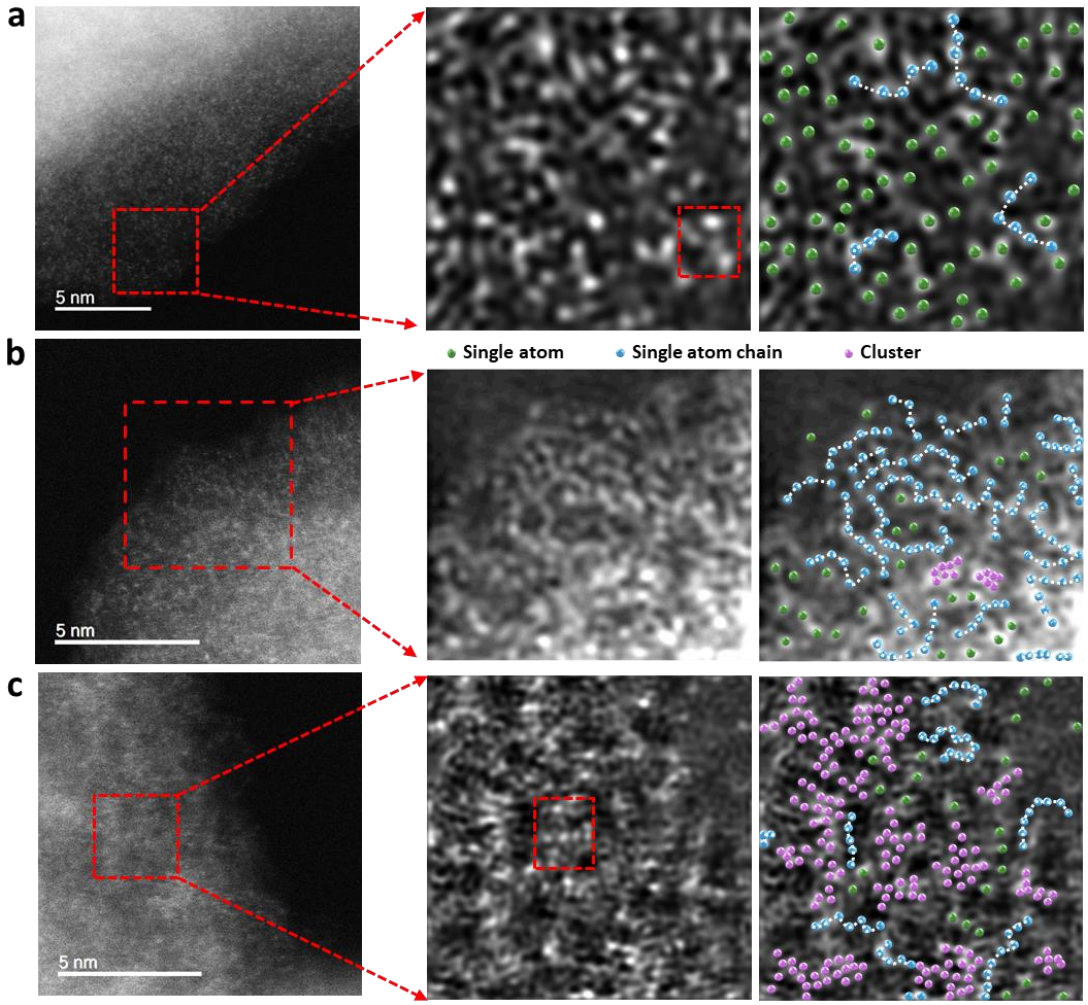

Figure S7. HAADF-STEM images of (a) Fe/NC/600, (b) Fe/NC/700 and (c) Fe/NC/800.

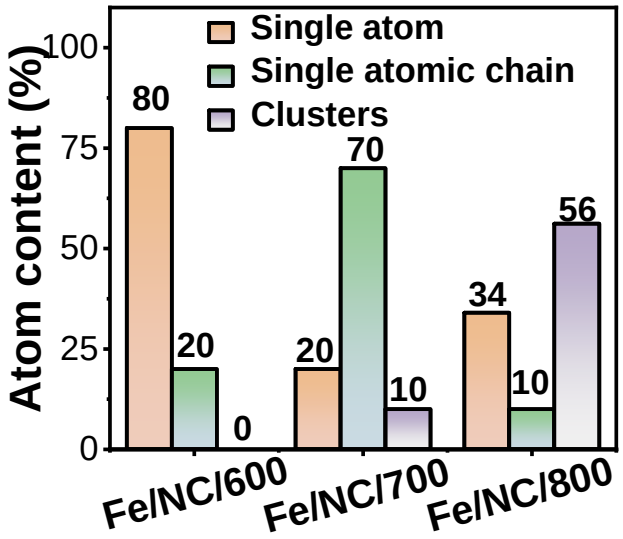

Figure S8. Percentages of single atom counts, atomic counts of single atom chains, and atomic counts of clusters relative to the total number of atoms in the selected region of Fe/NC/600, Fe/NC/700, and Fe/NC/800, respectively.

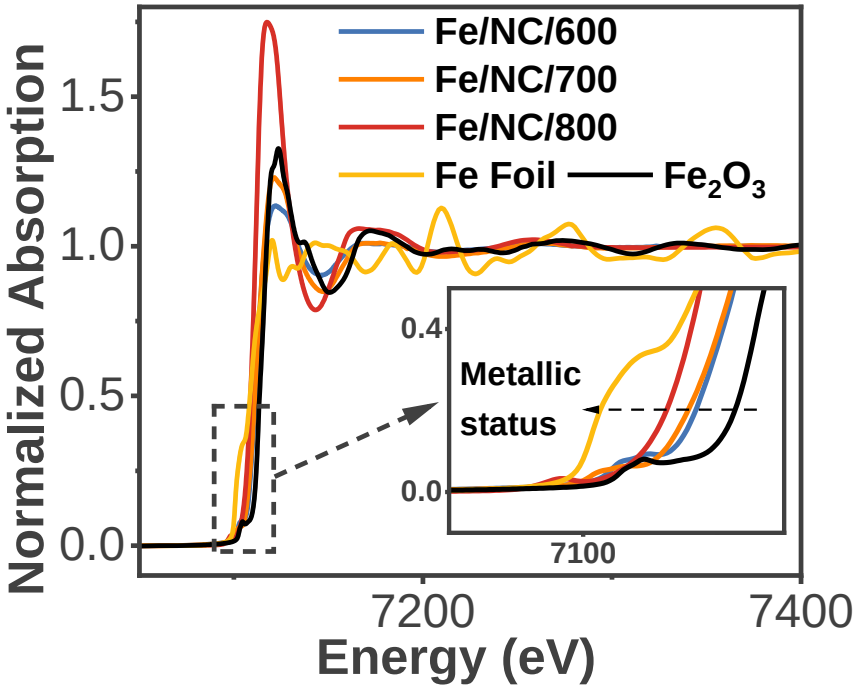

Figure S9. Normalized XANES spectra of Fe/NC/600, Fe/NC/700, Fe/NC/800, Fe_2O_3, and Fe foil at the K-edge.

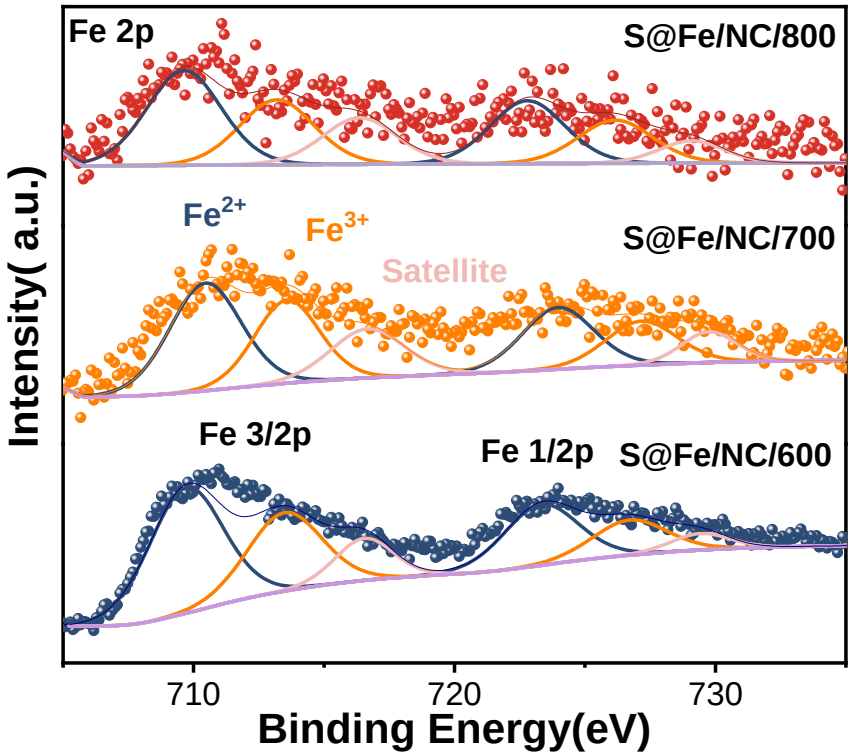

Figure S10. XPS spectra of the Fe 2p Peaks for S@Fe/NC/600, S@Fe/NC/700 and S@Fe/NC/800

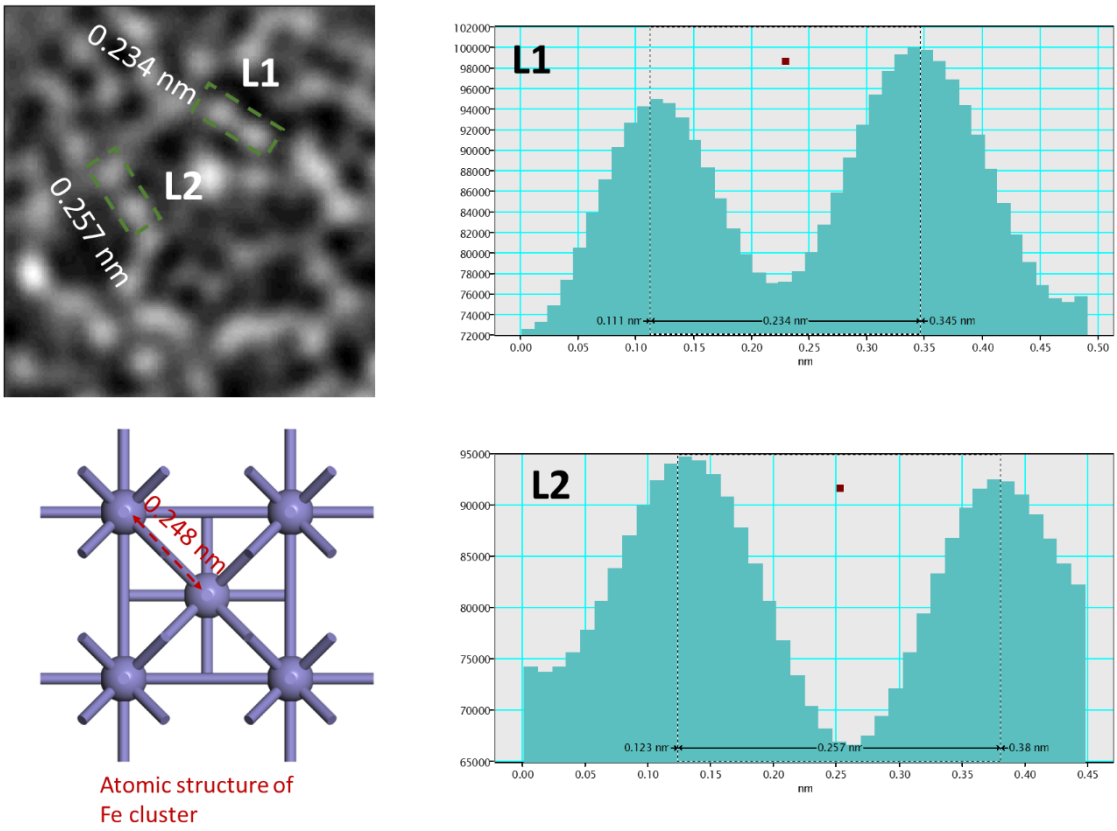

Figure S11. The measured Fe-Fe bond length (The right) of the selected Fe atom links in rectangle L1 and L2 (The top left), and the theoretical first-shell Fe-Fe bond length (The bottom left).

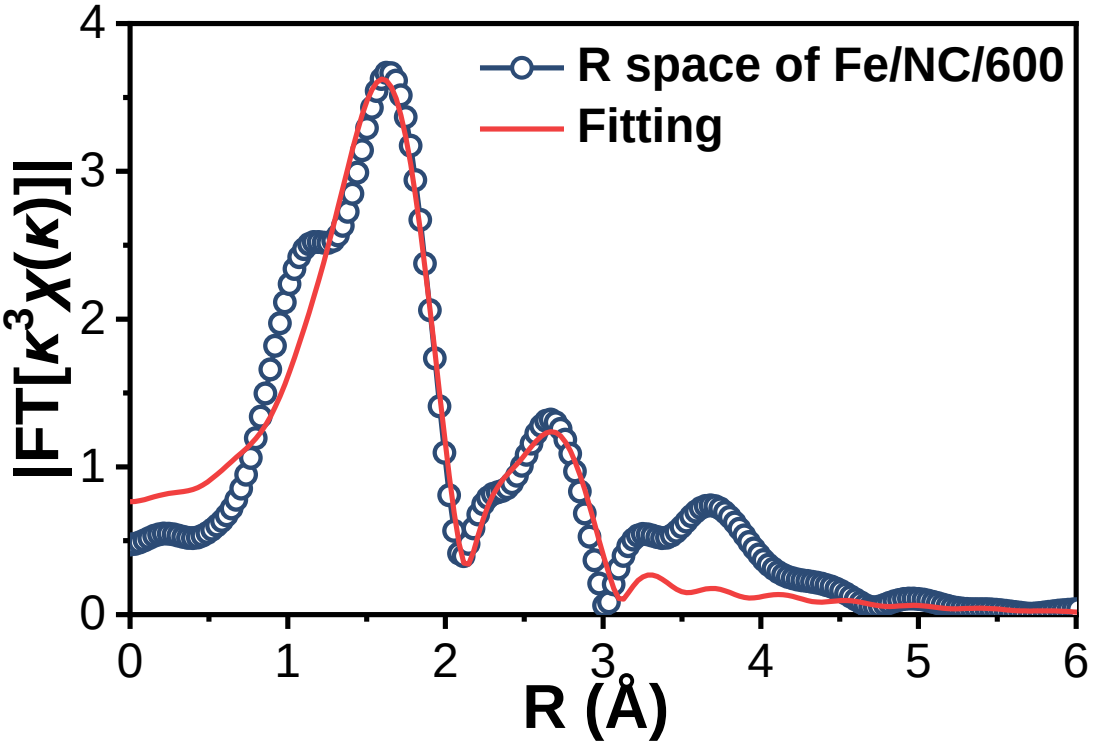

Figure S12. Corresponding Fe K-edge k^3-weighted FT-EXAFS fitting curve of Fe/NC/600 in R space. Data ranges: $3.0 \leq k \leq 10.3 Å^{-1}$, $1.0 \leq R \leq 3.0$ Å.

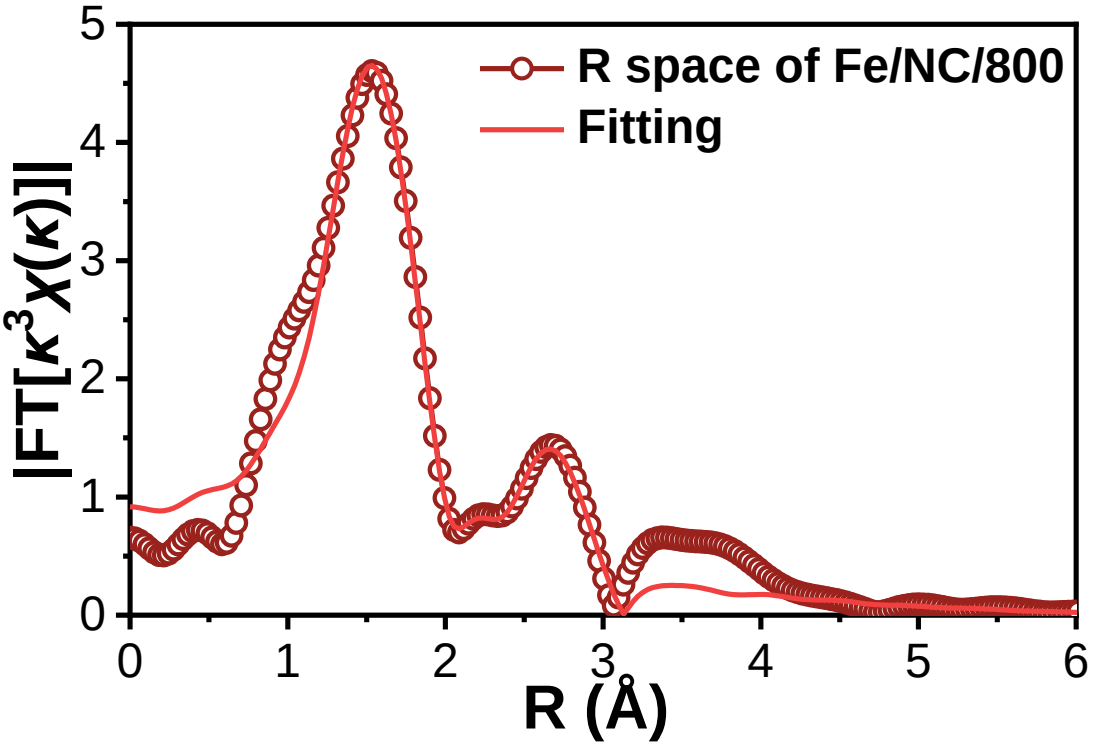

Figure S13. Corresponding Fe K-edge k^3-weighted FT-EXAFS fitting curve of Fe/NC/800 in R space. Data ranges: $3.0 \leq k \leq 10.1 Å^{-1}$, $1.0 \leq R \leq 3.0$ Å.

Table S1. EXAFS fitting parameters at the Fe K-edge for various samples (S_0^2=0.892).

Sample	Shell	N^a	R (Å)[b]	σ^2 (Å^2)[c]	ΔE_0 (eV)[d]	R factor
Fe/NC/600	Fe-N	2.3	1.92	0.010	4.9	0.006
	Fe-(N)-Fe	0.6	2.96	0.010		
Fe/NC/700	Fe-N	3.0	1.94	0.007	7.3	0.0027
	Fe-(N)-Fe	2.2	2.99	0.007		
Fe/NC/800	Fe-N	2.3	1.96	0.006	8.2	0.0033
	Fe-(N)-Fe	3.0	3.03	0.010		

S_0^2 is the amplitude reduction factor, which was obtained by fitting the standard Fe_2O_3 reference and then kept fixed when fitting the data of all samples. [a]*N*: coordination number; [b]*R*: bond distance; [c] σ^2: Debye-Waller factor; [d] ΔE_0: the inner potential correction. R factor: goodness of fit. S_0^2: path amplitude, set to 0.892, according to the experimental EXAFS fit of the Fe foil reference by fixing coordination numbers at the known crystallographic value.

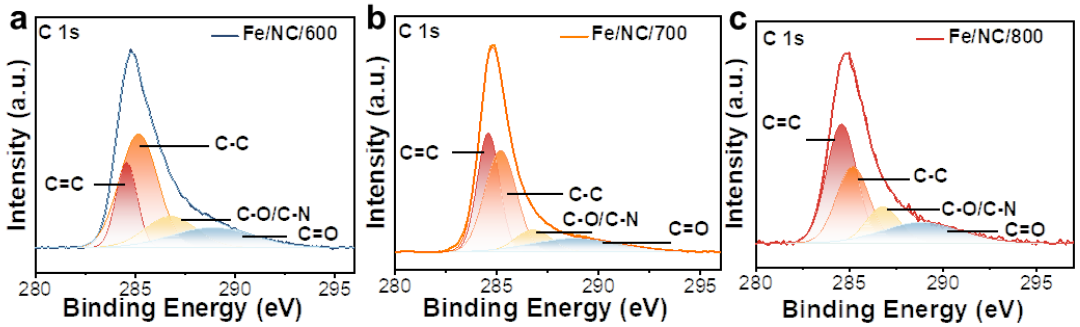

Figure S14. a-c) C 1s XPS spectra for Fe/NC/600, Fe/NC/700, and Fe/NC/800.

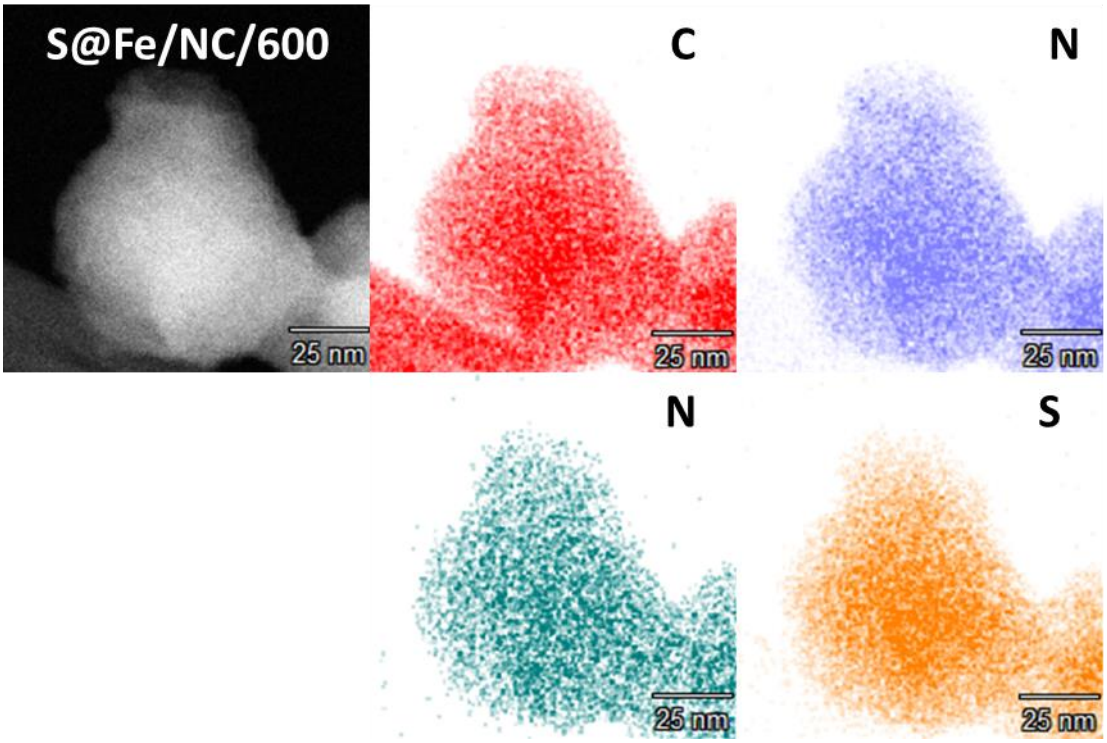

Figure S15. EDS mapping of S@Fe/NC/600

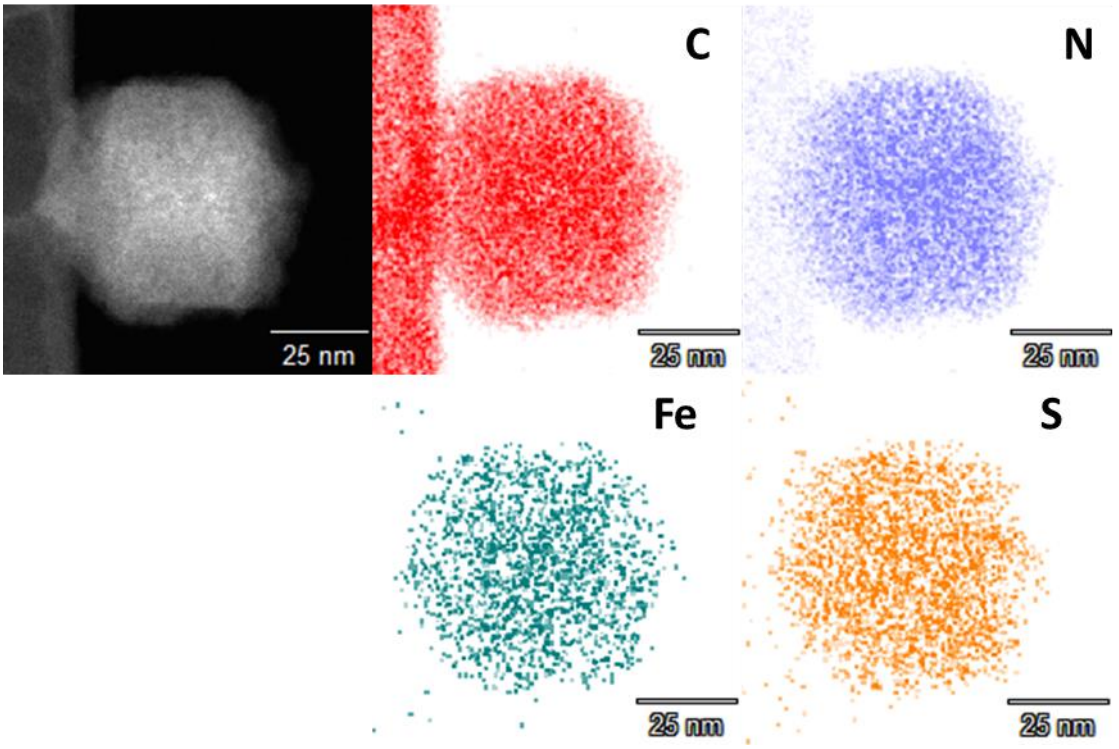

Figure S16. EDS mapping of S@Fe/NC/700

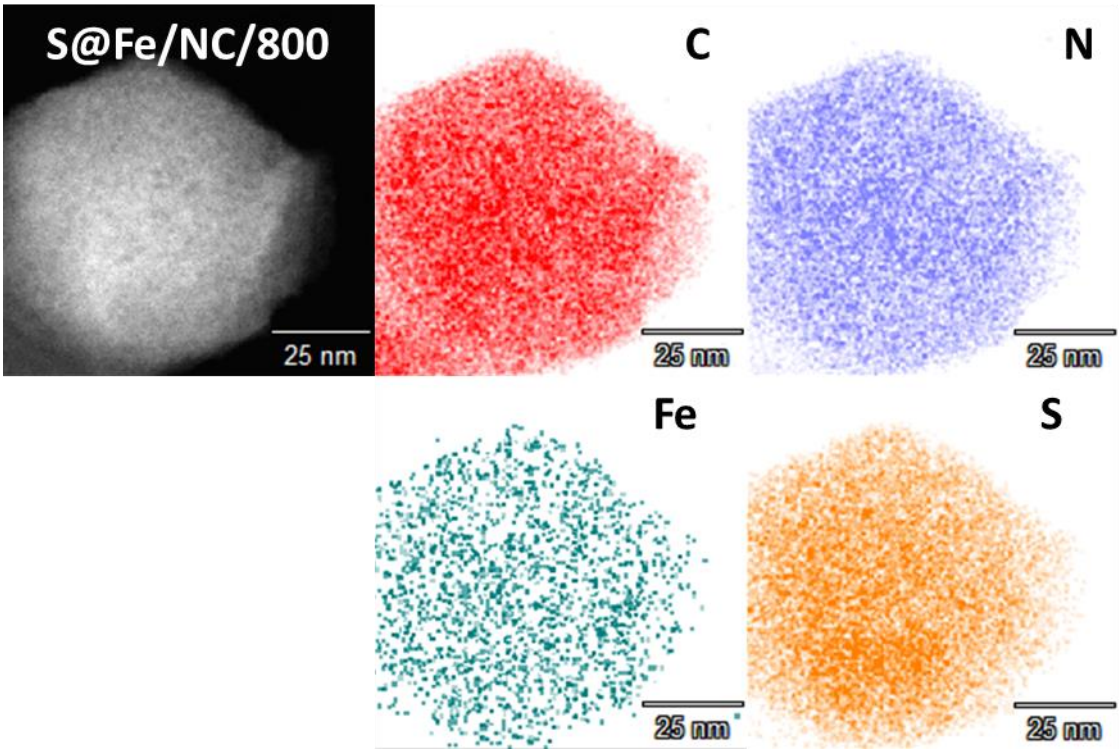

Figure S17. EDS mapping of S@Fe/NC/800

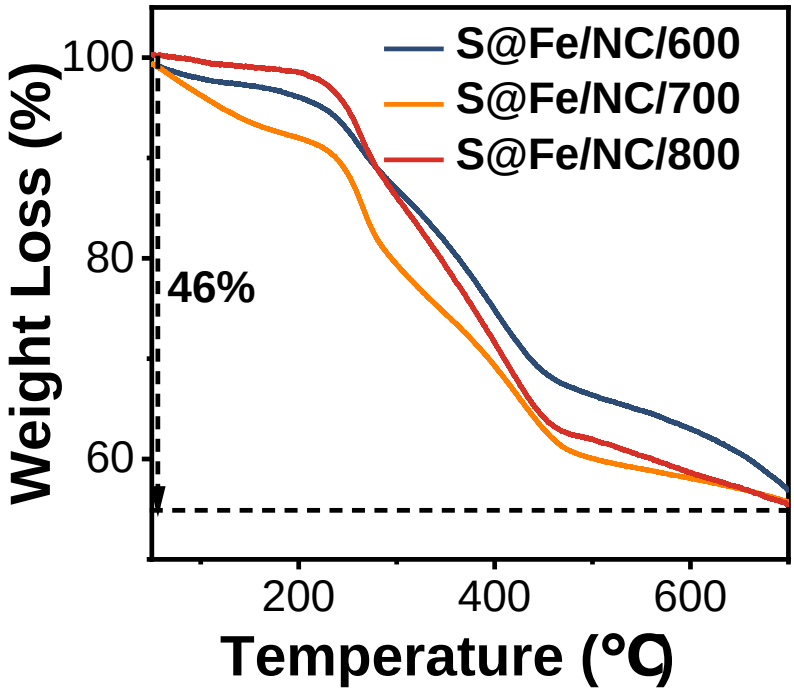

Figure S18. TGA curves for S@Fe/NC/600, S@Fe/NC/700, and S@Fe/NC/800.

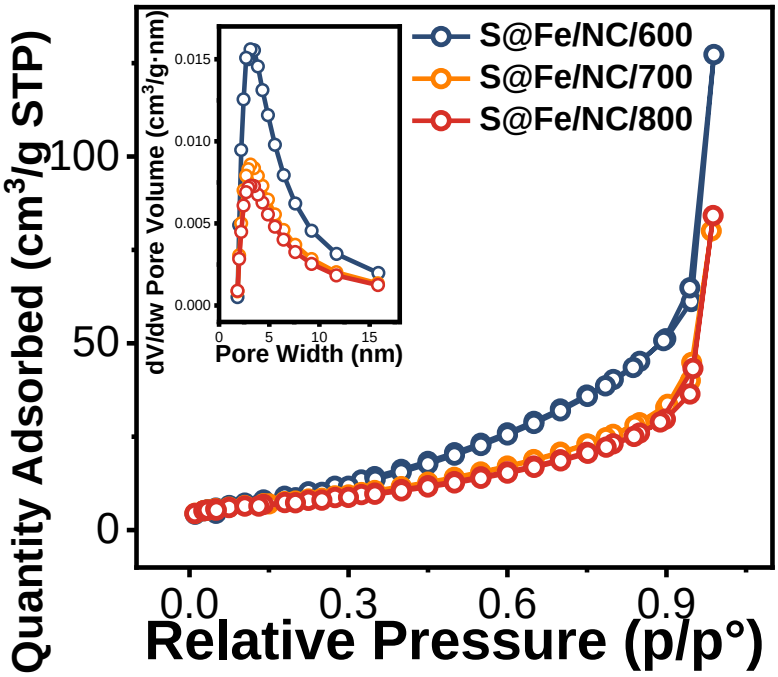

Figure S19. BET isotherms of S@Fe/NC/600, S@Fe/NC/700, and S@Fe/NC/800, respectively, with the corresponding pore size distributions in the inset.

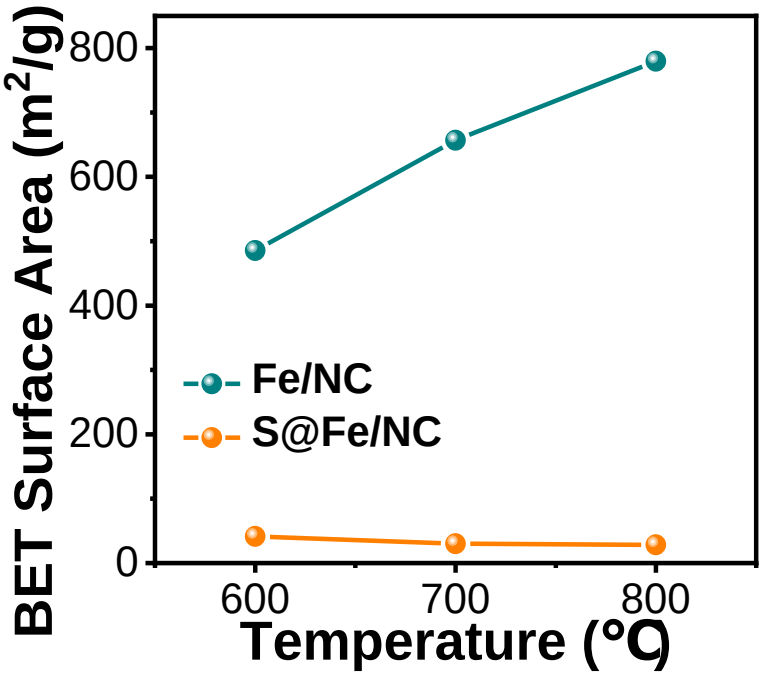

Figure S20. Surface areas of Fe/NC/600, Fe/NC/700, and Fe/NC/800 before and after loading with S.

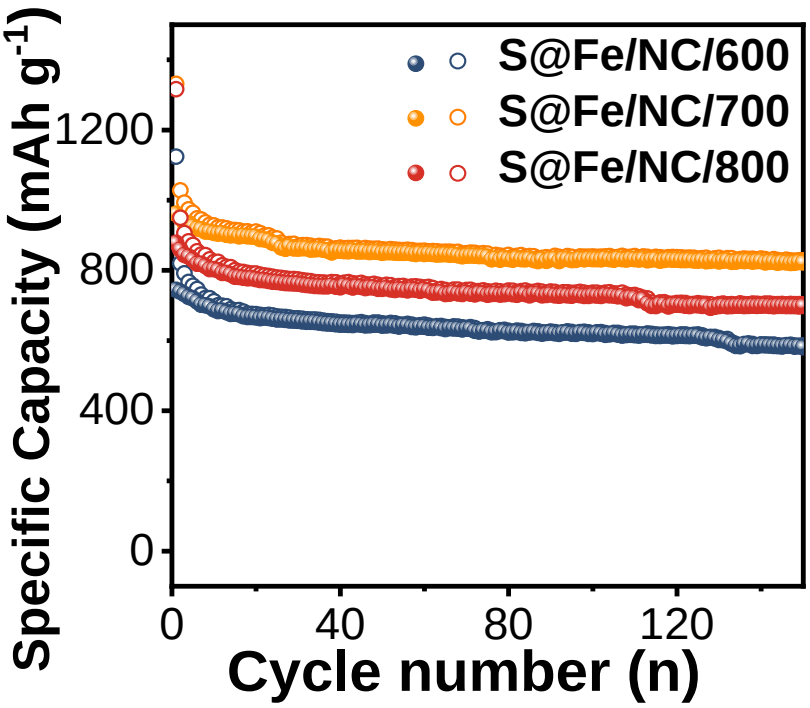

Figure S21. Cycling stability of S@Fe/NC/600, S@Fe/NC/700, and S@Fe/NC/800 at the current density of 0.2 A g^{-1}.

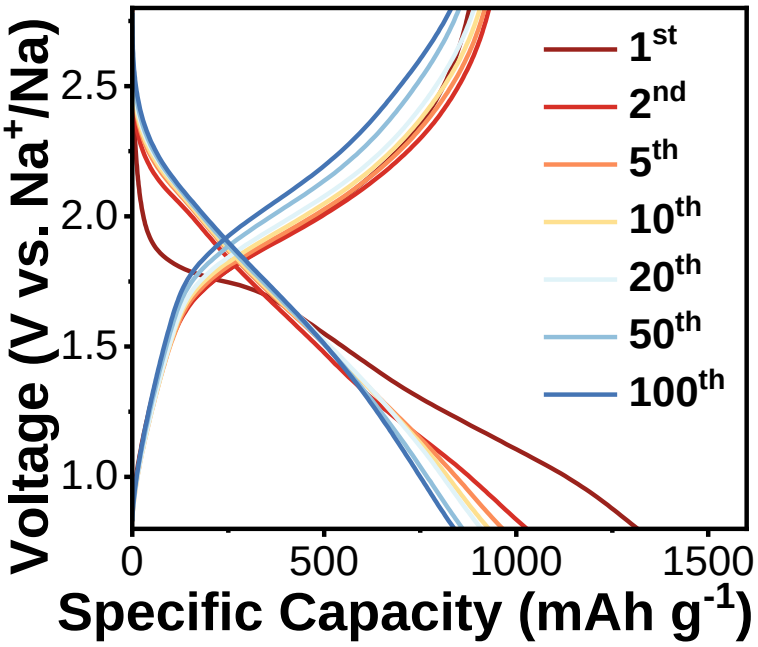

Figure S22. Specific capacity of S@Fe/NC/700 at different cycles at the current density of 0.2A g^{-1}.

Table S2. Summary of electrochemical performances in previous references.

Samples	Sufur content	Mass Loading(cm^2 g^{-1})	Electrolyte	Voltage (V vs. Na/Na^+)	Rate performance	Cycling performance	Ref.
S@Fe/NC/700	47%	1.5-2	1 M $NaClO_4$ in EC/PC	0.8-2.8	300 mAh·g^{-1} at 20 A·g^{-1}	Retained 380 $mAhg^{-1}$ after 5000 cycles at 10 A·g^{-1}	This work
MMPCS-800@S	43.8%	-	1 M $NaClO_4$ in EC/PC+5%FEC	0.8-2.8	544 mAh·g^{-1} at 5 Ag^{-1}	Retained 420 mAh·g^{-1} after 2000 cycles at 2 A· g^{-1}	Ref 1. [1]
S/MoC@NHC-15	52%	2-3	1 M $NaClO_4$ in EC/DEC	0.5-2.8	398.4 mAh·g^{-1} at 5 C	Retained 250 mAh·g^{-1} after 1000 cycles at 5 C	Ref 2. [2]
S@Co_1-CoS_2/NC	54%	1.6	1 M $NaClO_4$ in EC/PC+5%FEC	0.8-2.8	441 mAh g^{-1} at 5 A g^{-1}	Retained 358 mAh g^{-1} after 5000 cycles at 5 A g^{-1}	Ref 3. [3]
3D-PNCV@S	44.4%	-	1 M NaTFSI in PC/FEC	0.8-3	471 $mAhg^{-1}$ at 5Ag^{-1}	Retained 445$mAhg^{-1}$ after 800 cycles at 5Ag^{-1}	Ref 4. [4]
NiS_2@NPCTs/S	56%	2.5	1 M $NaClO_4$ in EC/PC+3%FEC	0.8-2.8	203 mAh·g^{-1} at 5 A·g^{-1}	401 mAh·g^{-1} after 750 cycles at 1 A·g^{-1}	Ref 5. [5]
Cu SA/NOC/S-2	67%	2-2.5	1 M $NaSO_3CF_3$ in DEGDME	0.8-2.8	483 mAh·g^{-1} at 5 A g^{-1}	601 mAh·g^{-1} after 1000 cycles at 1 A·g^{-1}	Ref 6. [6]
S@$FeNi_3$@HC	50.6%	-	2 M NaTFSI in PC/FEC	0.8-3	383 mAh·g^{-1} at 5 A g^{-1}	591 mAh·g^{-1} after 500 cycles at 2 A·g^{-1}	Ref 7. [7]
FeS_2@NCMS/S	65.5%	-	1 M $NaClO_4$ in EC/PC+3%FEC	0.5-2.8	139 mAh·g^{-1} at 5 A·g^{-1}	270 mAh·g^{-1} after 300 cycles at 0.1 A·g^{-1}	Ref 8. [8]
MOF-C/S/PDAc	37%	0.9-1.5	1 M $NaClO_4$ in PC+5%FEC	0.8-2.8	304 mAh·g^{-1} at 10 A·g^{-1}	680 mAh·g^{-1} after 500 cycles at 1 A·g^{-1}	Ref 9. [9]
CN/Au/S	56.5%	-	1 M $NaClO_4$ in PC+5%FEC	0.8-2.8	181 mAh·g^{-1} at 20 A·g^{-1}	369 mAh·g^{-1} after 2000 cycles at 10 A g^{-1}	Ref 10. [10]

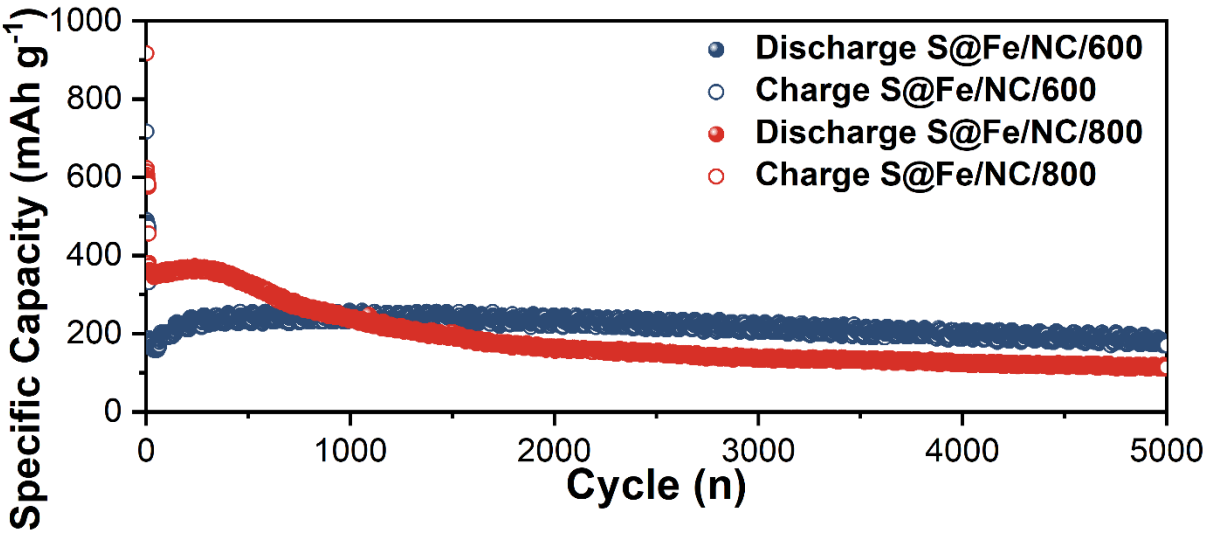

Figure S23. Long-term cycling stability of the S@Fe/NC/600 and S@Fe/NC/800 samples at the current density of 10 A g^{-1}.

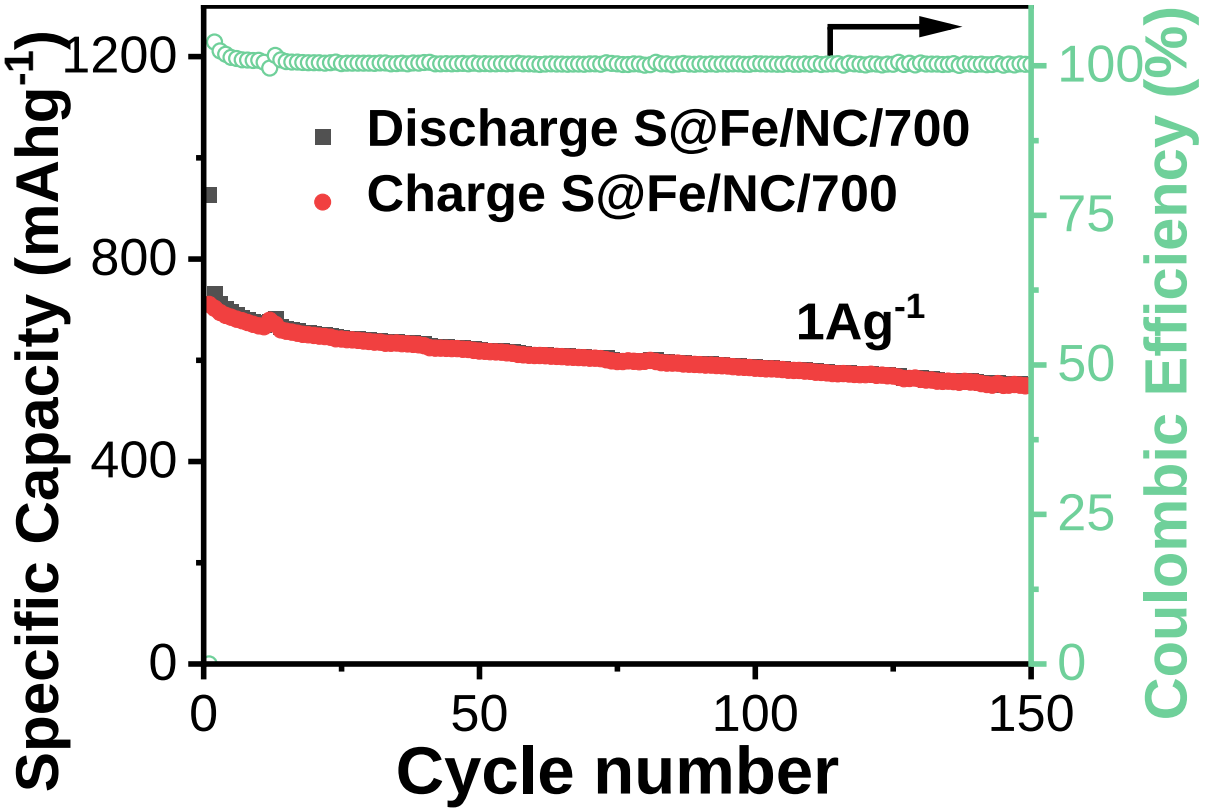

Figure S24. Cycling performance of S@Fe/NC/700 at the current density of 1 A g^{-1} with a high sulfur loading of 4.0-4.5 mg cm^{-2}.

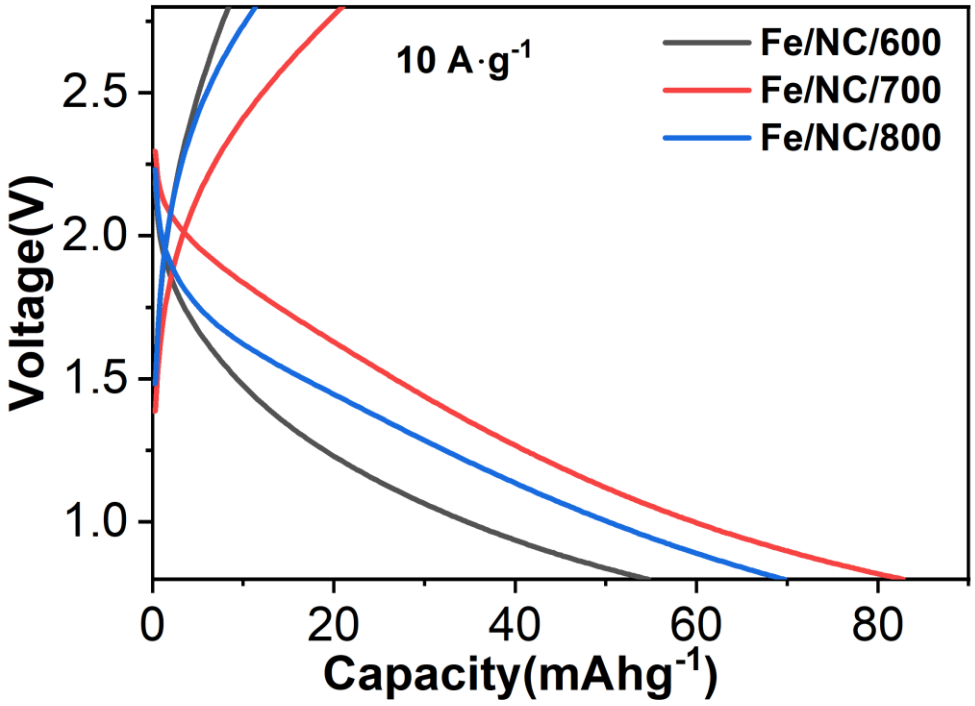

Figure S25. The sodium-ion performance of Fe/NC/600, Fe/NC/700, and Fe/NC/800 at 10 A g^{-1}.

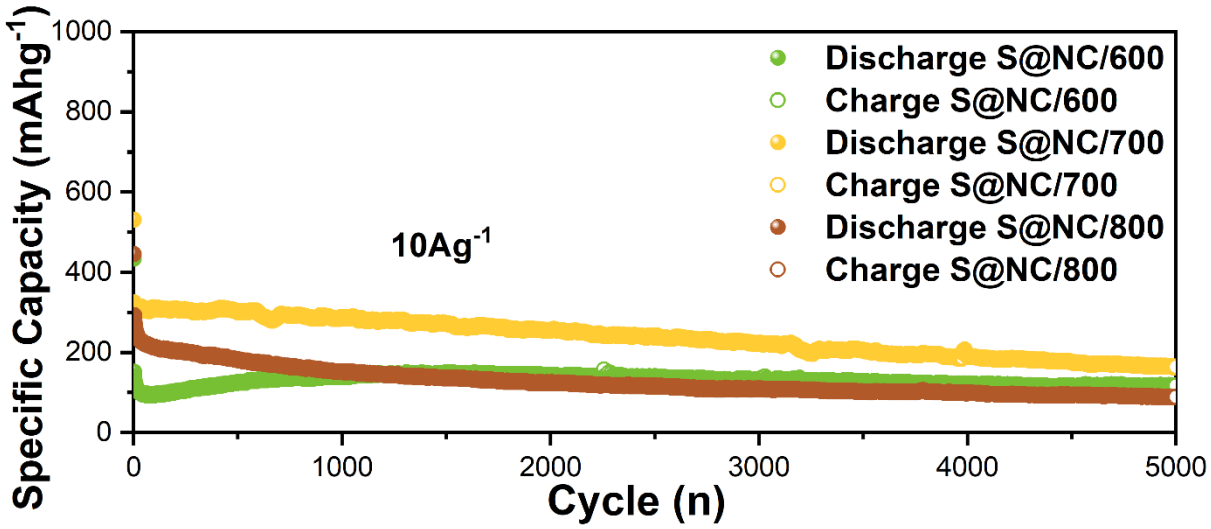

Figure S26. The performances of S@NC/600, S@NC/700, and S@NC/800 under a current density of 10 A g^{-1}.

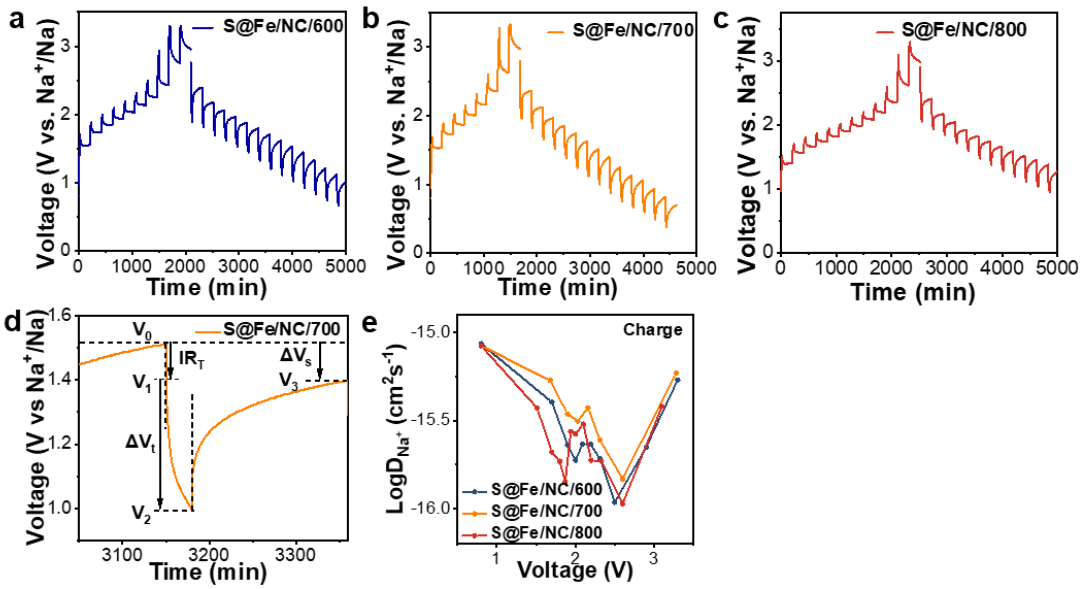

Figure S27. a-c) GITT curves of S@Fe/NC/600, S@Fe/NC/700, and S@Fe/NC/800, respectively. d) ΔV_t and ΔV_s are defined. e) Na-ion diffusion coefficients of S@Fe/NC/600, S@Fe/NC/700, and S@Fe/NC/800 calculated from the GITT data.

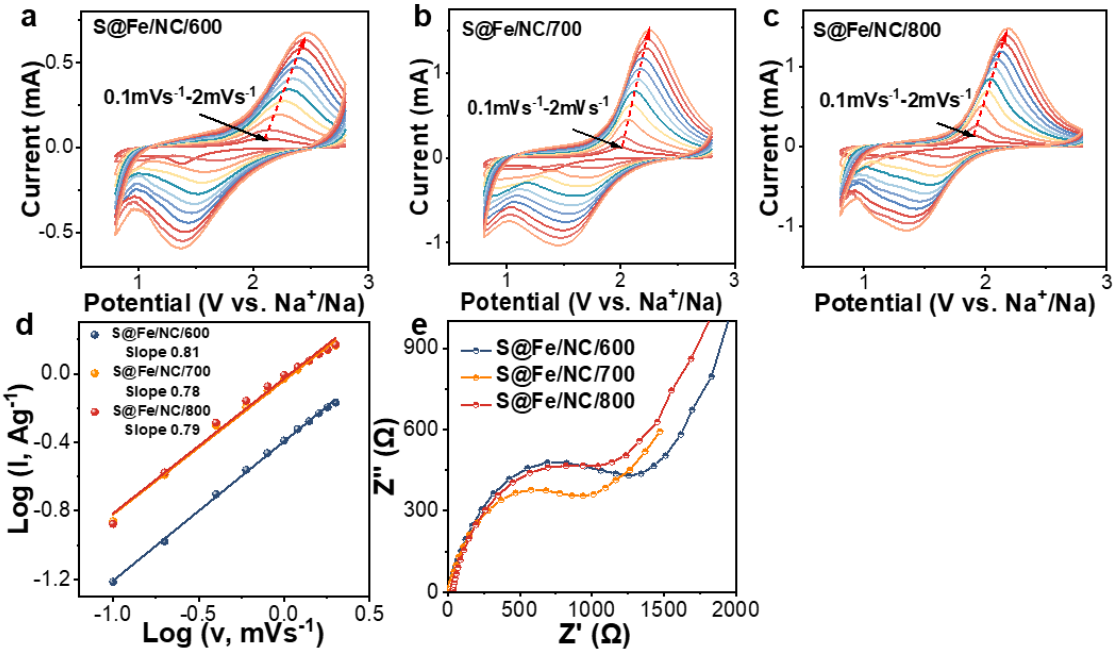

Figure S28. The CV curves of the (a) S@Fe/NC/600, (b) S@Fe/NC/700, and (c) S@Fe/NC/800 samples from 0.1 to 2.0 mV s^{-1}. (d) *b*-values (slopes) obtained from the current oxidation peaks, $i = av^b$ of the CV curves. (e) Nyquist plots for S@Fe/NC/600, (b) S@Fe/NC/700, and (c) S@Fe/NC/800 cells, respectively.

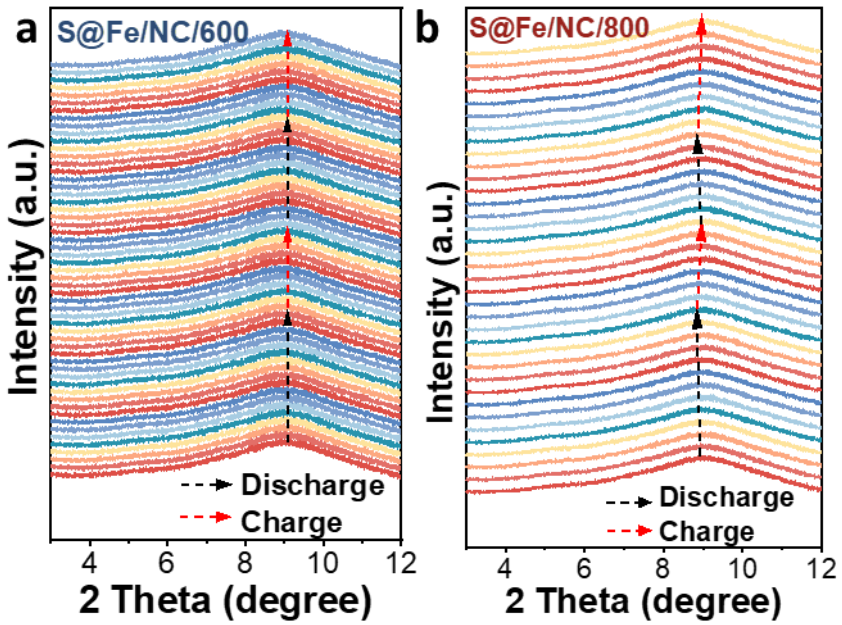

Figure S29. In-situ XRD patterns of S@Fe/NC/600 and S@Fe/NC/800.

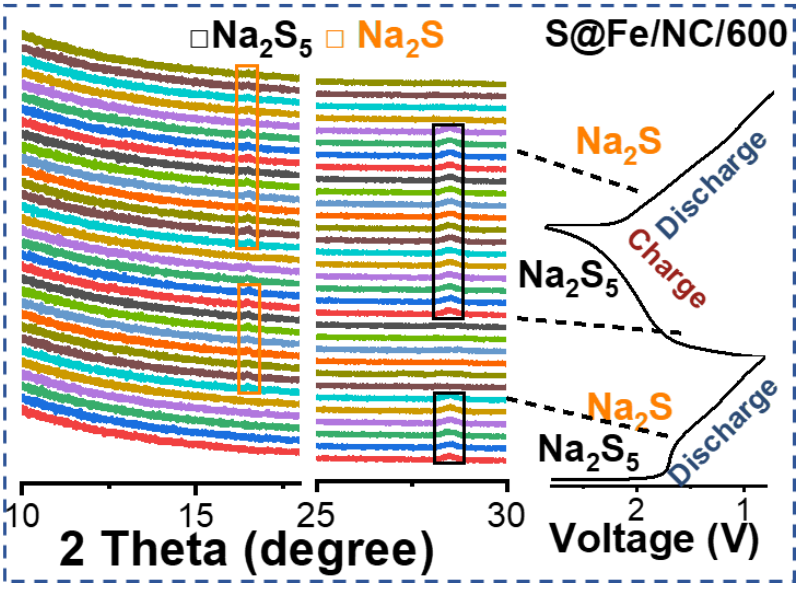

Figure S30. In-situ synchrotron XRD patterns and corresponding discharge/charge curves of S@Fe/NC/600.

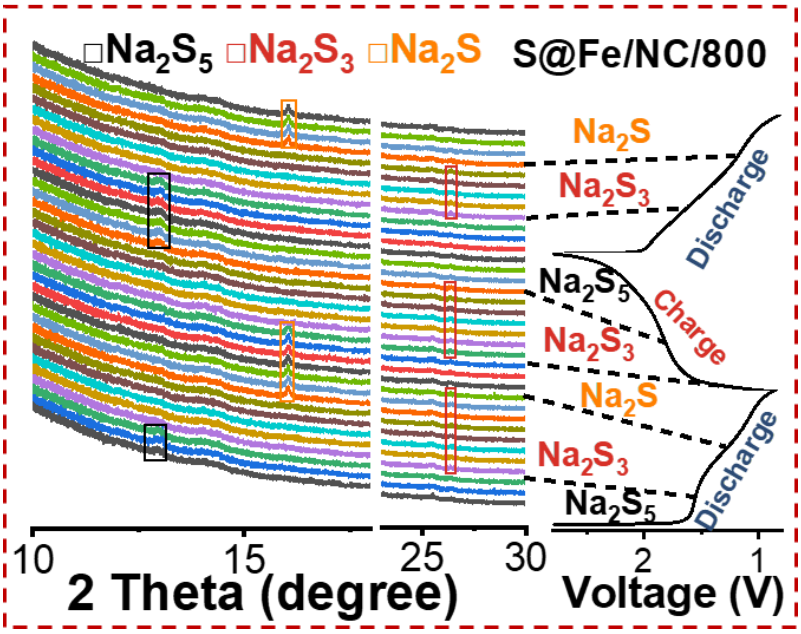

Figure S31. In-situ synchrotron XRD patterns and corresponding discharge/charge curves of S@Fe/NC/800.

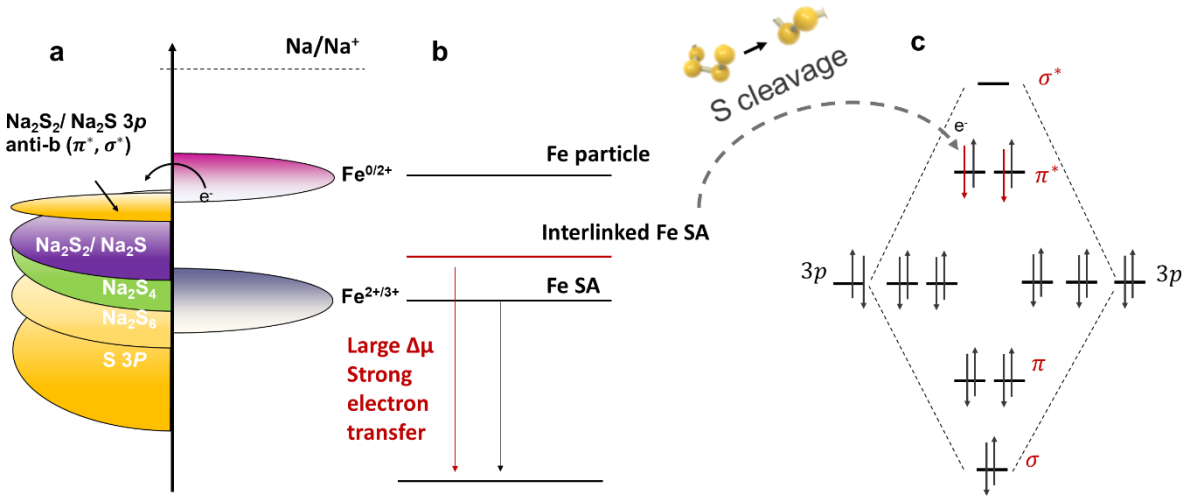

Figure S32. (a) Schematic illustration of electron transfer caused by change in the electronic structure, where the voltage is determined by the energy gap. (b) Schematic illustration of potential driving force difference between Fe single atom and interlinked Fe single atoms. (c) Diagram of S-S orbital energy levels.

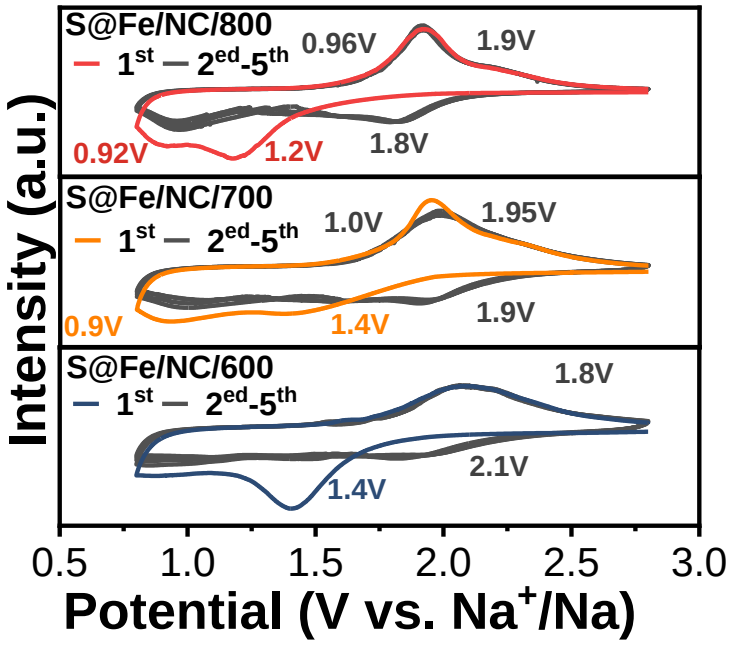

Figure S33. CV curves of the S@Fe/NC/600 and S@Fe/NC/800 under the scanning rate of 0.1 Vs^{-1}.

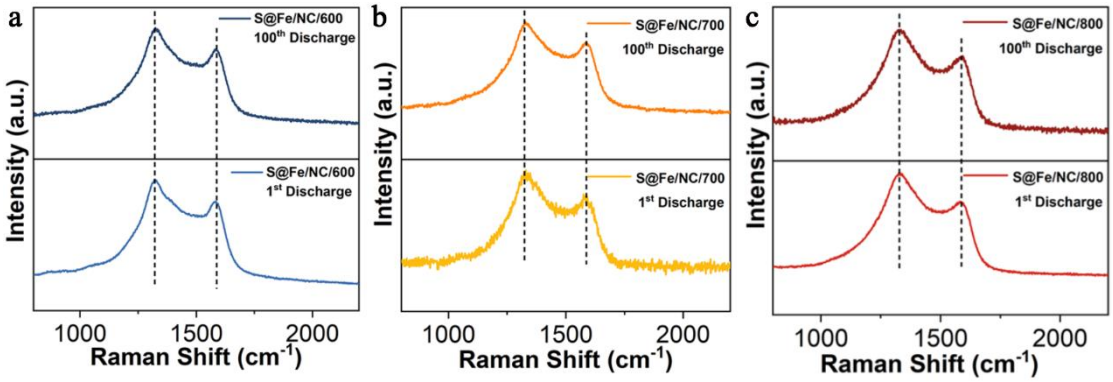

Figure S34. Raman spectra of S@Fe/NC/600, S@Fe/NC/700, and S@Fe/NC/800 after 100 cycles at the current density of 10 A g^{-1}.

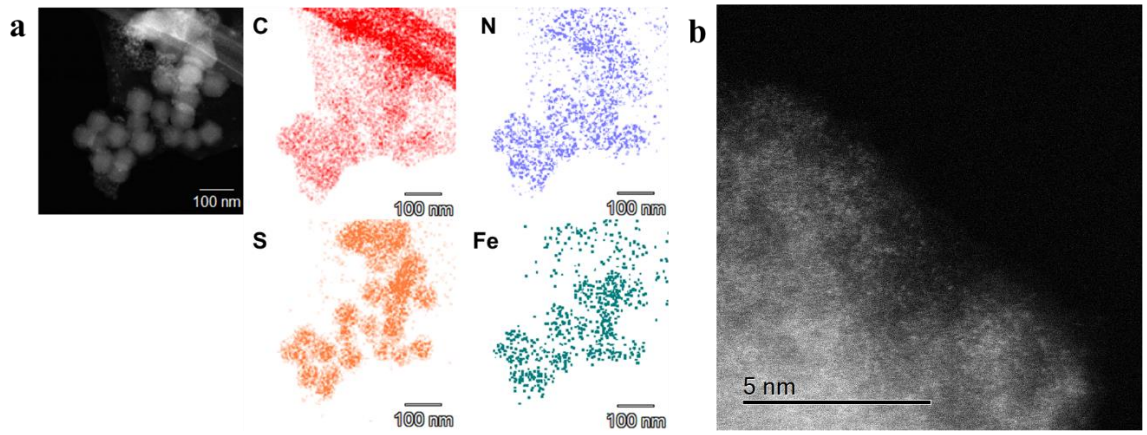

Figure S35. EDS mapping and HADDF-STEM for S@Fe/NC/700 after 200 cycles.

References

[1] C. Wu, Y. Lei, L. Simonelli, D. Tonti, A. Black, X. Lu, W. H. Lai, X. Cai, Y. X. Wang, Q. Gu, S. L. Chou, H. K. Liu, G. Wang, S. X. Dou, *Adv. Mater.* **2022**, 34, 2108363.

[2] J. Mou, Y. Li, L. Ou, J. J. E. S. M. Huang, **2022**, 52, 111.

[3] Y. Lei, C. Wu, X. Lu, W. Hua, S. Li, Y. Liang, H. Liu, W. H. Lai, Q. Gu, X. Cai, N. Wang, Y. X. Wang, S. L. Chou, H. K. Liu, G. Wang, S. X. Dou, *Angew. Chem., Int. Ed.* **2022**, 61.

[4] Y. Jiang, Z. Yu, X. Zhou, X. Cheng, H. Huang, F. Liu, H. Yang, Y. Yao, X. Rui, Y. Yu, *Adv. Mater.* **2022**, 2208873.

[5] Z. Yan, J. Xiao, W. Lai, L. Wang, F. Gebert, Y. Wang, Q. Gu, H. Liu, S.-L. Chou, H. Liu, S.-X. Dou, *Nat. Commun.* **2019**, 10.

[6] F. Xiao, H. Wang, J. Xu, W. Yang, X. Yang, D. Y. W. Yu, A. L. Rogach, *Adv. Energy Mater.* **2021**, 11, 2100989.

[7] L. Wang, H. Wang, S. Zhang, N. Ren, Y. Wu, L. Wu, X. Zhou, Y. Yao, X. Wu, Y. Yu, *ACS Nano* **2021**, 15, 15218.

[8] Z. Yan, Y. Liang, J. Xiao, W. Lai, W. Wang, Q. Xia, Y. Wang, Q. Gu, H. Lu, S. L. Chou, Y. Liu,
H. Liu, S. X. Dou, *Adv. Mater.* **2020**, 32, 1906700.

[9] F. Xiao, X. Yang, H. Wang, J. Xu, Y. Liu, D. Y. W. Yu, A. L. Rogach, *Adv. Energy Mater.* **2020**, 10, 2000931.

[10] N. Wang, Y. Wang, Z. Bai, Z. Fang, X. Zhang, Z. Xu, Y. Ding, X. Xu, Y. Du, S. Dou, G. Yu, *Energy Environ. Sci.* **2020**, 13, 562.